

Nonlinear State–Space Model of Semiconductor Optical Amplifiers With Gain Compression for System Design and Analysis

Scott B. Kuntze, Aaron J. Zilkie, *Member, IEEE, Student Member, OSA*,
Lacra Pavel, *Senior Member, IEEE, Member, OSA*, and J. Stewart Aitchison, *Senior Member, IEEE, Fellow, OSA*

Abstract—In this paper, we derive a new analytical state–space model for semiconductor optical amplifier (SOA) dynamics with nonlinear gain compression. We show that a multichannel closed-form state–space model is possible with polynomial gain compression and position-independent carrier density. The compressed model is significantly more accurate than existing noncompressed models as demonstrated by comparison with pump–probe experiments: response magnitude and recovery time are more accurately modeled with explicit gain compression. We then apply the model to design an optical feedback controller that regulates the total optical power at the output of a gain-compressed SOA.

Index Terms—Gain control, optical control, optical crosstalk, optical feedback, optical pulse measurements, power control, semiconductor optical amplifiers, state–space methods.

I. PURPOSE: ACCURATE DYNAMIC MODEL FOR SYSTEM DESIGN AND ANALYSIS

BECAUSE the semiconductor optical amplifier (SOA) is so versatile [1]–[5], it is the prime candidate for the active unit in next-generation integrated optical circuitry. As SOA-based photonic circuits become more complex, it becomes increasingly important to regulate their behavior for the circuits and receivers that follow downstream. In response, there is a growing collection of SOA control designs in the literature [6]–[10].

Input–output state–space models are particularly useful for SOA control design [6] as well as rapid system analysis [11] even if some approximations must be made for the sake of obtaining analytical closed-form expressions. State–space models are easily linearized to produce linear time-invariant systems for which there is a rich field of analysis and design (see [12] for example). The resulting controllers can be used to regulate and groom the output of single SOAs or complex photonic circuits. Furthermore, state–space models consist of sets of first-order ordinary differential equations, so system simulation is fast compared to finite-element models [11].

Manuscript received September 1, 2007; revised March 7, 2008. Current version published August 29, 2008.

The authors are with the Department of Electrical and Computer Engineering, University of Toronto, Toronto, ON M5S 3G4, Canada (e-mail: scott.kuntze@utoronto.ca; aaron.zilkie@utoronto.ca; pavel@control.utoronto.ca).

Digital Object Identifier 10.1109/JLT.2008.922212

Current SOA state–space models [6], [11] do not contain explicit gain compression, a strong nonlinear effect that suppresses the amplification dynamics and limits the maximum gain available [13], [14]. Nonlinear gain compression is an important factor in applications such as asymmetric demultiplexers [15], loop mirrors [16], cross-gain-modulation wavelength converters [17], logic gates [18], and bit shapers [19].

In this paper, we develop a multichannel SOA state–space model that includes gain compression for the first time; the phenomenological compression constant ϵ that we employ accounts for carrier heating and spectral hole burning [20], [21]. Furthermore, we demonstrate that our compressed model is significantly more accurate than the existing uncompressed state–space models [6], [11]. Our model can be adapted to complex control design and system analysis up to 100 GHz.

We start by deriving a generalized SOA state–space model in Section II. We then evaluate the forms of gain that permit closed-form solutions to the SOA photon propagation equation, and show that only polynomial compression yields a usable solution. In Section III, we verify the resulting compressed model against pump–probe experiments that elucidate carrier recovery and output dynamics: agreement between the model and experiments is very good, while prior noncompressed models overestimate both magnitude and time constant. Finally, in Section IV, we use the compressed model to design and demonstrate a constant feedback controller that regulates the total output power of a single SOA.

II. NONLINEAR STATE–SPACE MODEL DERIVATION

A. Governing Equations

The SOA governing equations consist of an optical power propagation equation for each optical channel $i = 0, 1, \dots, m$

$$\frac{\partial P_i(z, t)}{\partial z} = g_i(N, P, Q, z, t)P_i(z, t) - \alpha_i P_i(z, t) \quad (1)$$

a set of optical power propagation equations for discretized amplified spontaneous emission (ASE), $j = 1, \dots, \mu$

$$\frac{\partial Q_j^\pm(z, t)}{\partial z} = \pm(g_j(N, P, Q, z, t) - \alpha_j)Q_j^\pm(z, t) + \hbar\omega_j R_{sp,j}(N, z, t) \quad (2)$$

TABLE I
PARAMETER DEFINITIONS AND VALUES FOR THE MODELS AND SIMULATIONS
(ALL-OPTICAL CHANNELS ARE TAKEN TO BE IDENTICAL)

Parameter	Symbol	Value	Unit
Inversion carrier density	N	—	cm^{-3}
Active region current	I	—	mA
Total active region current	\bar{I}	—	mA
Nonradiative recombination rate	R	—	$\text{cm}^{-3}\text{s}^{-1}$
Linear recombination	R_A	2.9×10^8	s^{-1}
Bimolecular recombination	R_B	4.5×10^{-11}	cm^3s^{-1}
Auger recombination	R_C	1.5×10^{-29}	cm^6s^{-1}
Spontaneous radiation rate	R_{sp}	—	s^{-1}
Length	L	1	mm
Ridge width	W	2	μm
Active region height	H	150	nm
Active region area	A	$W \times H$	m^2
Active region volume	V	$A \times L$	m^3
Effective refractive index	n_{eff}	3.2	—
Data channel power	P	—	mW
Set of data channels	\mathbf{P}	—	mW
ASE channel power	Q_{\pm}	—	mW
Set of ASE channels	\mathbf{Q}	—	mW
Optical carrier number	m	—	—
ASE carrier number	μ	—	—
Optical carrier frequency	ω	$2\pi c/1560\text{e-9}$	rad/s
Single-pass gain	g	—	cm^{-1}
Con?nement & gain factor	$\Gamma\alpha$	75	cm^{-1}
Transparency carrier density	N_{tr}	5×10^{17}	cm^{-3}
Log gain parameter [?]	N_s	2.4×10^{17}	cm^{-3}
Waveguide loss	α	17	cm^{-1}

and a population inversion density rate equation

$$\begin{aligned} \frac{\partial N(z,t)}{\partial t} = & \frac{I(z,t)}{qV} - R(N,z,t) \\ & - \frac{1}{A} \sum_{i=0}^m \frac{g_i(N, \mathbf{P}, \mathbf{Q}, z, t) P_i(z, t)}{\hbar\omega_i} \\ & - \frac{2}{A} \sum_{j=1}^{\mu} \frac{g_j(N, \mathbf{P}, \mathbf{Q}, z, t) Q_j(z, t)}{\hbar\omega_j} \end{aligned} \quad (3)$$

with all parameters defined in Table I. The factor of 2 in the ASE recombination term accounts for power in both transverse modes [11], while the spontaneous emission R_{sp} is determined by the cavity modes [22], [23]

$$R_{\text{sp},j}(N, z, t) = n_{\text{sp},j}(N, z, t) g_j(N, \mathbf{P}, \mathbf{Q}, z, t) \Delta f_j \quad (4a)$$

$$= \frac{N(z, t) g_j(N, \mathbf{P}, \mathbf{Q}, z, t) c}{(N(z, t) - N_{\text{tr},j})(2n_{\text{eff},j}L)} \quad (4b)$$

The discretization of the ASE spectrum need not necessarily imply the presence of resonant cavity modes—there can be as many discrete ASE channels as is necessary to represent the broadband noise spectrum of the device, as well as the broadband effect of ASE on the carrier population outside the data channel bandwidths.

To produce an input–output state–space model, we must integrate each of these equations over the length L of the SOA.

B. General State–Space Form

A state–space model consists of a system of first-order ordinary differential equations $\dot{\mathbf{x}}(t) = \mathbf{f}(\mathbf{x}(t), \mathbf{u}(t))$ that keep track of how the states $\mathbf{x}(t)$ change due to inputs $\mathbf{u}(t)$ through functions \mathbf{f} , along with output relations $\mathbf{y}(t) = \mathbf{h}(\mathbf{x}(t), \mathbf{u}(t))$ that

determine the outputs $\mathbf{y}(t)$ due to $\mathbf{x}(t)$ and $\mathbf{u}(t)$ through functions \mathbf{h} . We proceed by casting the governing SOA equations into this state–space form. Rearranging the propagation equations (1) and (2), we have

$$g_i(N, \mathbf{P}, \mathbf{Q}, z, t) P_i(z, t) = \left(\alpha_i + \frac{\partial}{\partial z} \right) P_i(z, t) \quad (5)$$

and

$$g_j(N, \mathbf{P}, \mathbf{Q}, z, t) Q_j^{\pm} = \left(\pm \frac{\partial}{\partial z} + \alpha_j \right) Q_j^{\pm} \mp R_{\text{sp},j}(N, z, t). \quad (6)$$

Substituting (5) and (6) into the stimulated emission terms of the rate equation (3), we get

$$\begin{aligned} & \frac{\partial N(z,t)}{\partial t} \\ = & \frac{I(z,t)}{qV} - R(N,z,t) - \frac{1}{A} \sum_{i=0}^m \frac{1}{\hbar\omega_i} \left[\frac{\partial}{\partial z} + \alpha_i \right] P_i(z,t) \\ & - \frac{2}{A} \sum_{j=1}^{\mu} \frac{1}{\hbar\omega_j} \left(\left[\frac{\partial}{\partial z} + \alpha_j \right] Q_j^+(z,t) + \left[\frac{\partial}{\partial z} + \alpha_j \right] Q_j^-(z,t) \right). \end{aligned} \quad (7)$$

Integrating on $z \in [0, L]$ and normalizing by L gives

$$\begin{aligned} & \frac{d\bar{N}(t)}{dt} \\ = & \frac{\bar{I}(t)}{qV} - \bar{R}(N, t) \\ & - \frac{1}{A} \sum_{i=0}^m \left[\frac{P_i(L, t) - P_i(0, t)}{\hbar\omega_i L} + \frac{\alpha_i \bar{P}_i(t)}{\hbar\omega_i} \right] \\ & - \frac{2}{A} \sum_{j=1}^{\mu} \left(\left[\frac{Q_j^+(L, t) - Q_j^+(0, t)}{\hbar\omega_j L} + \frac{\alpha_j \bar{Q}_j^+(t)}{\hbar\omega_j} \right] \right. \\ & \left. + \left[\frac{Q_j^-(L, t) - Q_j^-(0, t)}{\hbar\omega_j L} + \frac{\alpha_j \bar{Q}_j^-(t)}{\hbar\omega_j} \right] \right) \end{aligned} \quad (8)$$

where the overbars indicate length-averaged quantities, for example

$$\bar{P}_i(t) \triangleq \frac{1}{L} \int_0^L P_i(z, t) dz. \quad (9)$$

For (8) to be useful in producing a state–space model, it must have an analytical closed form, so there must exist analytical closed-form solutions for $P_i(z, t)$ and $Q_j^{\pm}(z, t)$. Hence, the solutions to (1) and (2) (the output relations) and (8) (the state update equation) constitute the general state–space form for any set of gains $\mathbf{g}(N, \mathbf{P}, \mathbf{Q}, z, t)$, with state $\bar{N}(t)$, inputs $\mathbf{P}(0, t)$ and $\mathbf{Q}^{\pm}(0, t)$, and outputs $\mathbf{P}(L, t)$ and $\mathbf{Q}^{\pm}(L, t)$.

C. Solving the Propagation Equation With Gain Compression

For rational gain compression [13] in the multichannel case, we have for each channel i

$$\frac{\partial P_i(z,t)}{\partial z} = \frac{g_i(N, z, t) P_i(z, t)}{1 + \epsilon_i [P_i(z, t) + \Sigma_i(z, t)]} - \alpha_i P_i(z, t) \quad (10)$$

where ϵ_i is the gain compression factor that accounts for spectral hole burning and carrier heating [20], [21], and where

$$\Sigma_i(z, t) \triangleq \sum_{\substack{k=0 \\ k \neq i}}^m P_k(z, t) + \sum_{j=1}^{\mu} [Q_j^+(z, t) + Q_j^-(z, t)] \quad (11)$$

is used to emphasize that the sum of remaining channels $k \neq i$ and ASE is an unknown function in z . Equation (10) is an ordinary differential equation in z , specifically an Abel equation of the second type, class A. Although certain forms of Abel equations are analytically solvable, to our knowledge this particular one (10) has no analytical closed-form solution due to the presence of the $\Sigma_i(z, t)$ term, even with clever algebraic rearrangement as in the appendix of [25]. Even if we restrict the model to only one single channel or total optical power, (10) reduces to

$$\frac{\partial P(z, t)}{\partial z} = \frac{g(N, z, t)P(z, t)}{1 + \epsilon P(z, t)} - \alpha P(z, t) \quad (12)$$

which again is an Abel equation (second type, class A) without a closed-form solution.

Because rational gain compression is analytically intractable, we turn to polynomial gain compression [13] in the multichannel case with form

$$\frac{\partial P_i(z, t)}{\partial z} = g_i(N, z, t)P_i(z, t)(1 - \epsilon_i[P_i(z, t) + \Sigma_i(z, t)]) - \alpha_i P_i(z, t) \quad (13)$$

where again (11) is used for the remaining channels $k \neq i$ and ASE. This ordinary differential equation in z (13) is a Bernoulli equation that has an analytical solution, but the solution contains indefinite integrals without explicitly known integrands in $g_i(N, z, t)$ and $\Sigma_i(z, t)$, and therefore cannot be used to find a definite $P_i(z, t)$; the indefinite integrals persist even in the single-channel case with $\Sigma_i(0, t) \equiv 0$.

From the previous analysis, we conclude that two assumptions are necessary to include nonlinear gain compression in a state-space model. The first assumption is that $N(z, t) = N(t)$ so that $g(N, z, t) = g(N, t)$. Because the final state-space form collapses the SOA into a lumped input-output device, this first assumption is not restrictive to our model. The second assumption is that gain compression acts via the inversion level density $\bar{N}(t)$ and that direct coupling via $\Sigma_i(z, t)$ can be ignored. This second assumption is potentially more restrictive, but the compression factors ϵ_i could be exaggerated to compensate for the additional compression contributed by the other signal channels. Furthermore, a single channel can be used to represent the total power of several channels if the channels have roughly equal operating parameters and the gain dispersion over their frequency span is relatively flat. With these two assumptions the solution to the propagation equation (13) is

$$P_i(z, t) = P_i(0, t)(g_i(N, t) - \alpha_i) \times \left[(g_i(N, t) - \alpha_i)e^{-[g_i(N, t) - \alpha_i]z} + \epsilon_i(1 - e^{-[g_i(N, t) - \alpha_i]z})g_i(N, t)P_i(0, t) \right]^{-1} \quad (14)$$

which is definite and therefore usable with the carrier rate (8). Note that when $\epsilon_i = 0$, we recover the output relation

$$P_i(z, t) = P_i(0, t)e^{[g_i(N, t) - \alpha_i]z} \quad (15)$$

which is the uncompressed model of [6]. Using (14), the average power levels in the SOA are

$$\bar{P}_i(t) = \frac{1}{\epsilon_i g_i(N, t)L} \times \ln \left[1 + \frac{\epsilon_i g_i(N, t)(e^{[g_i(N, t) - \alpha_i]L} - 1)P_i(0, t)}{g_i(N, t) - \alpha_i} \right]. \quad (16)$$

Because length integration collapses the SOA into a length-symmetric lumped device, forward and backward propagating ASE powers are indistinguishable inside the cavity. Hence, we take $Q_j(z, t) \triangleq Q_j^+(z, t) = Q_j^-(z, t)$ for $z \in (0, L)$. The solution for $Q_j(z, t)$ is obtained from (2) with the same assumptions as for $P_i(z, t)$

$$Q_j(z, t) = \frac{G_j(N, t) + \zeta_j(N, t)\varphi_j(N, z, t)}{2\epsilon_j g_j(N, t)} \quad (17)$$

where

$$G_j(N, t) \triangleq g_j(N, t) - \alpha_j \quad (18a)$$

$$\zeta_j(N, t) \triangleq \sqrt{4\epsilon_j g_j(N, t)R_{sp,j}(N, t) + G_j^2(N, t)} \quad (18b)$$

$$\varphi_j(N, z, t) \triangleq \tanh \left[\frac{z\zeta_j(N, t)}{2} + \operatorname{arctanh} \left(\frac{\xi_j(N, t)}{\zeta_j(N, t)} \right) \right] \quad (18c)$$

$$\xi_j(N, t) \triangleq 2\epsilon_j g_j(N, t)Q_j(0, t) - G_j(N, t). \quad (18d)$$

Averaging over the device length, we have

$$\bar{Q}_j(t) = \left[\frac{1}{L} \ln \left(\frac{\left[\frac{\xi_j(N, t)}{\zeta_j(N, t)} + 1 \right] \left[\frac{\xi_j(N, t)}{\zeta_j(N, t)} - 1 \right]}{[\varphi_j(N, L, t) + 1][\varphi_j(N, L, t) - 1]} \right) + G_j(N, t) \right] \times \frac{1}{2\epsilon_j g_j(N, t)}. \quad (19)$$

D. State-Space Model

The final state-space model consists of the $m + 1$ output relations

$$P_i(L, t) = P_i(0, t)(g_i(N, t) - \alpha_i) \times \left[(g_i(N, t) - \alpha_i)e^{-[g_i(N, t) - \alpha_i]L} + \epsilon_i(1 - e^{-[g_i(N, t) - \alpha_i]L})g_i(N, t)P_i(0, t) \right]^{-1} \quad (20)$$

and μ ASE equations

$$Q_j(L, t) = \frac{G_j(N, t) + \zeta_j(N, t)\varphi_j(N, L, t)}{2\epsilon_j g_j(N, t)} \quad (21)$$

along with the state update equation

$$\begin{aligned} \frac{d\bar{N}(t)}{dt} = & \frac{\bar{I}(t)}{qV} - \bar{R}(N, t) \\ & - \frac{1}{A} \sum_{i=0}^m \left(\frac{P_i(L, t) - P_i(0, t)}{\hbar\omega_i L} + \frac{\alpha_i \bar{P}_i(t)}{\hbar\omega_i} \right) \\ & - \frac{4}{A} \sum_{j=1}^{\mu} \left(\frac{Q_j(L, t) - Q_j(0, t)}{\hbar\omega_j L} + \frac{\bar{Q}_j(t)}{\hbar\omega_j} \right) \end{aligned} \quad (22)$$

which contains (16) and (19)–(21).

Single-pass gains $g_i(N, t)$ are often taken to be linear in the literature

$$g_i(\bar{N}, t) = \Gamma_i a_i (\bar{N}(t) - N_{\text{tr},i}) \quad (23)$$

although logarithmic forms are more accurate over the full range of carrier densities [24]

$$g_i(\bar{N}, t) = \Gamma_i a_i \ln \left[\frac{\bar{N} + N_{s,i}}{N_{\text{tr},i} + N_{s,i}} \right]. \quad (24)$$

In these gains, Γ is the modal confinement fraction, a is the incremental gain parameter, N_{tr} is the transparent carrier density, and N_s is a fitting parameter [24]; each parameter may be varied over the channels i to model spectral gain dispersion. Similarly, nonradiative recombination may assume the simpler form

$$\bar{R}(\bar{N}, t) = \frac{\bar{N}(t)}{\tau_c} \quad (25)$$

where a single recombination time constant τ_c is used, or the more complete form [24]

$$\bar{R}(\bar{N}, t) = R_A \bar{N}(t) + R_B \bar{N}^2(t) + R_C \bar{N}^3(t) \quad (26)$$

where $R_{A,B,C}$ are recombination coefficients. We are now ready to verify and apply this new state-space model described by (20)–(22).

III. MODEL VERIFICATION

Here, we employ pump-probe experiments and simulations to verify the accuracy of the state-space model. The data from pump-probe experiments are richer than digital pulse experiments because they reveal system dynamics over a wider range of time scales and are not limited by modulator rise times or detector bandwidths.

A. Experiment and Simulation

The essential aspects of the pump-probe experiment are conveyed in the schematic Fig. 1; the complete experiment configuration is described in detail in [26]. A Ti:sapphire-pumped optical parametric oscillator produced a train of nearly transform-limited laser pulses (150 fs full width half maximum, 13-ns period) at 1560 nm. The pulses were split into high-energy pump and low-energy probe pulses that were then frequency-shifted from each other so that they could be distinguished at the detector. For each pump-probe pulse pair, the pump pulse entered the SOA first and induced an impulse response; the following

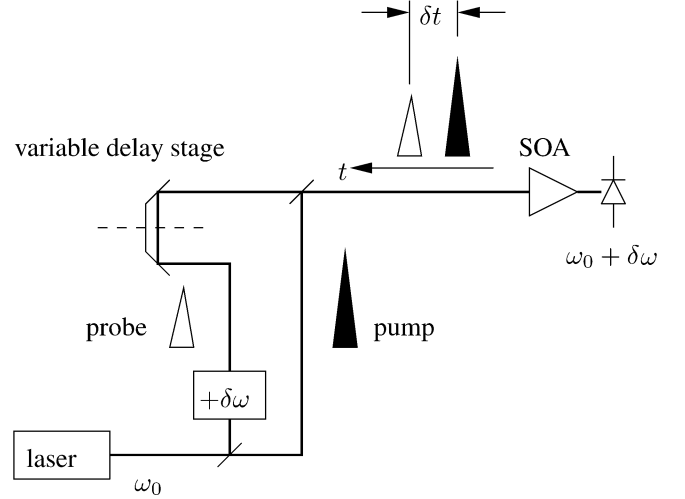


Fig. 1. Essential components of the pump-probe experiment necessary for state-space simulation.

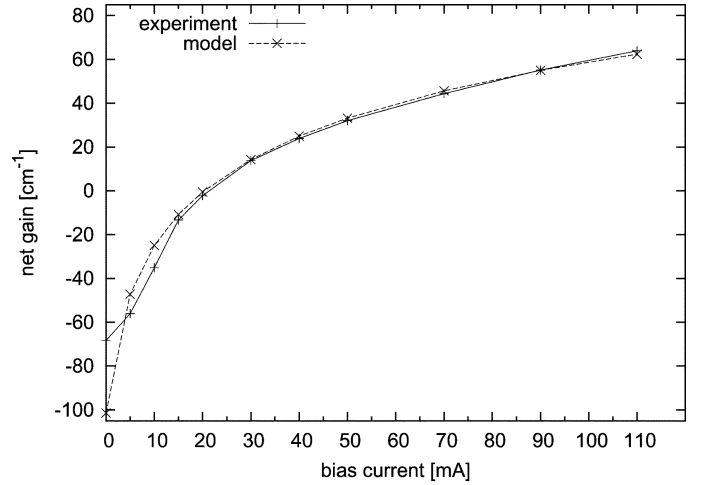


Fig. 2. Experimental and simulated gain curves of a multiquantum-well SOA. The gain parameters Γa , N_{tr} , and N_s are adjusted so that the calculated gain matches the experimental gain.

probe pulse was then variably delayed and its relative transmission used to measure the output and carrier dynamics of the SOA due to the pump pulse. Accounting for the insertion loss of the SOA, the pump pulse delivered approximately 1 pJ of energy at the input while the probe pulse delivered 0.1 pJ [27]. We verified our state-space model by replicating these essential experimental elements in simulation. Using a 2-ps window about the center of each pump pulse, the rate equation (22) was integrated with a resolution of 10 fs over a duration of 1.5 ns to produce a complete time response of the SOA induced by injected pump pulses at a given bias. Then, at 10-ps increments across the 1.5 ns of the pump response, we carried out delayed probe integrations using the pump response's inversion density $\bar{N}(t = \delta t - 1 \text{ ps})$ as the initial state for each probe integration (2-ps windows were employed about the centers of the probe pulses). The outputs were calculated with the output relation (20). ASE was modeled with a single ASE channel. This simulation method is fast and efficient by leveraging the state-space model and its capability of setting initial states.

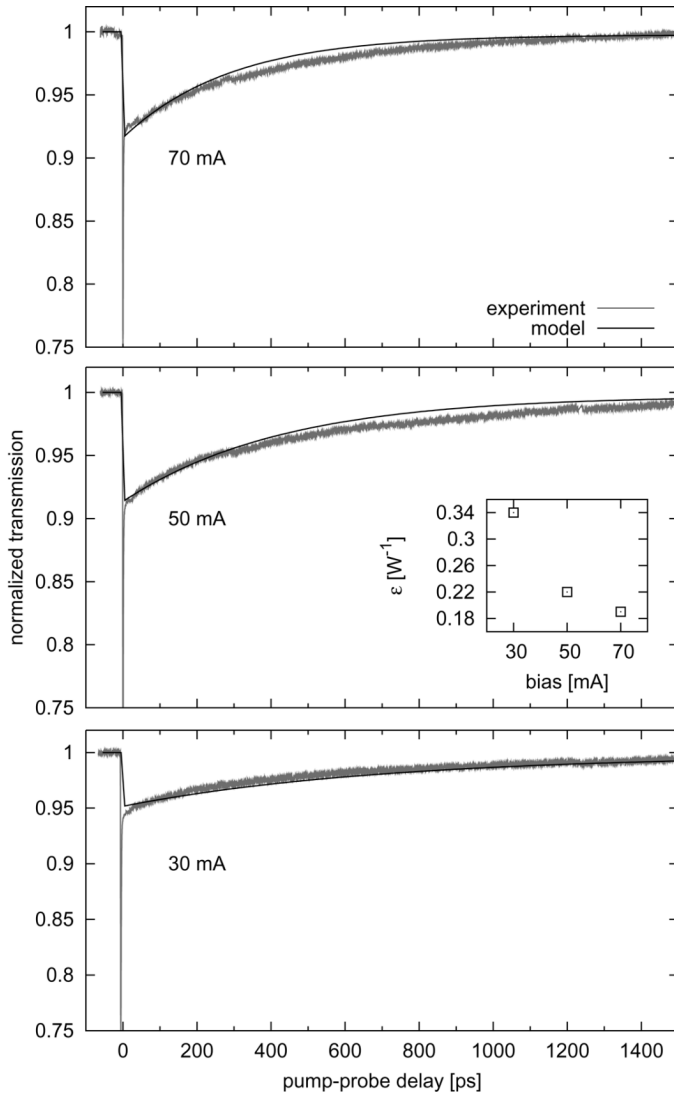


Fig. 3. Experimental and simulated pump-probe responses of a multi-quantum-well SOA at bias currents of 30, 50, and 70 mA. Inset: bias-dependent values of gain compression ϵ used to fit the model.

B. Device and Model Parameters

The SOA under test was an antireflection-coated multi-quantum-well ridge-waveguide architecture with five $\text{In}_{0.805}\text{Ga}_{0.195}\text{As}_{0.8}\text{P}_{0.2}$ active layers and $\text{In}_{0.805}\text{Ga}_{0.195}\text{As}_{0.405}\text{P}_{0.595}$ barriers grown by chemical beam epitaxy on an InP substrate [27]. Its electroluminescence peak was near 1560 nm as determined by measurements of its ASE spectrum [27]. The remaining physical dimensions and parameters are given in Table I. To match the model parameters to the experimental device, we first matched the net gain curves as a function of bias current as shown in Fig. 2. In the laboratory, net gain was measured by comparing input and output pulse magnitudes at very low input powers within the linear regime of the SOA. For the model, we set the input power to zero, found the equilibrium carrier density \bar{N}_0 , and then calculated

$$g_{\text{net}}(\bar{N}) = g(N, t) - \alpha \quad (27)$$

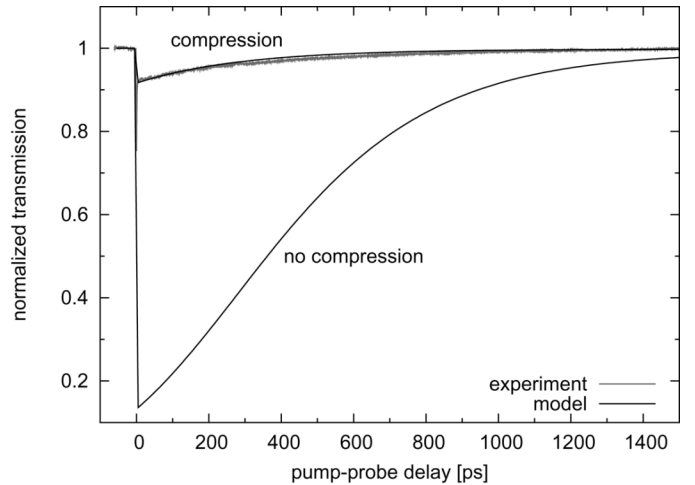


Fig. 4. Comparison of compressed and noncompressed state-space models of [6] (with ASE added) and [11] at 70 mA. The compressed model achieves a significantly better fit with experiment when the gain curves of Fig. 2 are properly matched over the gain regime.

where $g(N, t)$ is the single-pass gain of the sole signal channel using the logarithmic gain form (24). We then used the coefficients of the polynomial nonradiative recombination (26) and the gain compression factor ϵ as fitting parameters in the pump-probe simulation to set the magnitude and time constant of the response: increasing ϵ dampens the magnitude and slows the time constant, while increasing R_A (and to a lesser extent R_B and R_C) has the opposite effect. If the gain curve fit was upset, we iterated until suitable gain curve and pump-probe fits were obtained; the final values are listed in Table I.

There is some disagreement between the observed and simulated gain curves at low bias: the observed gain curve exhibits an inflection point around 10 mA. We attribute this low-bias disagreement to diode parasitics and current leakage [28] effects that are pronounced below threshold and that are not modeled—the quantity $\bar{I}(t)$ we set is the direct active region current and is not subject to parasitic electronic effects. However, there is excellent fit over the positive gain regime where the SOA would normally operate.

C. Experiment-Model Comparison

Fig. 3 shows general experiment-model agreement over a range of bias points. In the gain regime, the response magnitudes and recovery time constants agree well between experiment and simulation; fitted values of ϵ are shown in the inset. The initial spikes in the experimental data that last ≤ 1 ps are due to instantaneous two-photon absorption and ultrafast carrier heating, phenomena not captured in the governing SOA equations nor the resulting state-space model. However, up to 100 GHz, the state-space model performs extremely well.

By contrast, Fig. 4 demonstrates the inadequate modeling by the noncompressed models of [6] (with ASE added) and [11] at 70 mA: with the gain curve fit of Fig. 2, the noncompressed model greatly overestimates the response magnitude and recovery time constant compared to the compressed model. Similar overestimations are present at the other bias points.

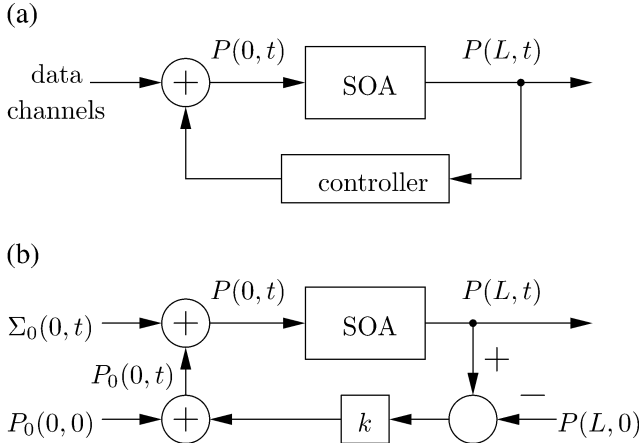


Fig. 5. Feedback controller using total input–output optical powers: (a) general control scheme, and (b) constant output feedback controller simulated in Fig. 6.

IV. OPTICAL FEEDBACK CONTROL FOR CONSTANT OUTPUT POWER

With the compressed model qualified, we apply it to design a controller that regulates total output power to protect devices and detectors downstream from power transients. We have shown [6] that maintaining constant output power keeps the inversion carrier density constant, which, in turn, decouples the data channels and suppresses interchannel crosstalk; a controller operating on total input and output powers in a multi-channel system will have the same effect even if the individual channels are not resolved by the controller.

Fig. 5(a) illustrates a general total-power control scheme. The total power is measured at the output, sent to the control circuit, and the resulting control signal is added to the data channels on a separate control channel $P_0(0, t)$ so that the total input power into the SOA is

$$P(0, t) = \Sigma_0(0, t) + P_0(0, t). \quad (28)$$

Fig. 6 shows a numerical integration of the compressed model's response to a series of 20% and 40% optical modulations (representing one and two-channel adds/drops for a group of five channels) as shown in Fig. 6(c) when using the constant feedback controller of Fig. 5(b)

$$P_0(0, t) = P_0(0, 0) + k[P(L, t) - P(L, 0)]. \quad (29)$$

With this constant feedback, the output power is given by

$$P(L, t) = \frac{(f_b - f_c) + \sqrt{(f_b - f_c)^2 + 4f_a f_d}}{2f_d} \quad (30)$$

where

$$f_a = G(N, t)[\Sigma_0(0, t) + P_0(0, 0) - kP(L, 0)] \quad (31a)$$

$$f_b = kG(N, t) \quad (31b)$$

$$f_c = G(N, t)e^{-G(N, t)L} + \frac{\epsilon g(N, t)f_a[1 - e^{-G(N, t)L}]}{G(N, t)} \quad (31c)$$

$$f_d = k\epsilon g(N, t)[1 - e^{-G(N, t)L}]. \quad (31d)$$

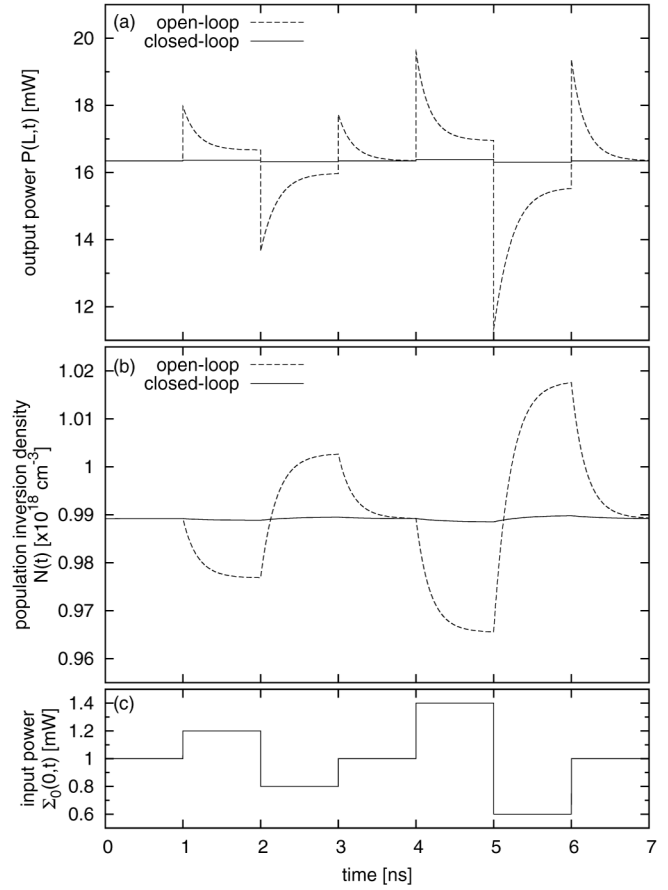


Fig. 6. Regulation of the total output power, using the control scheme of Fig. 5(b) with constant controller $k = -10$: (a) total optical output, (b) inversion carrier density, and (c) data channel optical input.

We design $k = -10$ for $\Sigma_0(0, 0) = P_0(0, 0) = 1$ mW; the bias current is set to a constant 70 mA. The total output power in Fig. 6(a) is kept relatively constant because the population inversion density in Fig. 6(b) is held constant by the optical feedback channel, despite data channel adds/drops in Fig. 6(c). This controller could be realized by tapping off a small percentage of the output light, collecting it with a broadband photodetector, and driving a laser of frequency $\omega_{i=0}$ through a high-speed differential amplifier [29] with a reference calibrated to a desired output $P(L, 0)$.

V. CONCLUSION

In summary, a new SOA state–space model with polynomial gain compression was derived from a generalized state–space model. The model behaved as expected in comparison with the previously verified uncompressed model—gain was suppressed and recovery time increased. The compressed model achieved significantly better agreement to experimental pump–probe data than previous noncompressed models. We employed the model to design an output power regulator that maintained a relatively constant output power despite disturbances at the input. This model could be used to design and analyze a variety of control schemes or evaluate communication system performance.

REFERENCES

- [1] Z. Bakonyi, G. Onishchukov, C. Knoll, M. Golles, and F. Lederer, "10 Gbit/s RZ transmission over 5000 km with gain-clamped semiconductor optical amplifiers and saturable absorbers," *Electron. Lett.*, vol. 36, pp. 1790–1791, Oct. 2000.
- [2] C. R. Doerr, L. W. Stulz, R. Pafchek, K. Dreyer, and L. Zhang, "Potentially low-cost widely tunable laser consisting of a semiconductor optical amplifier connected directly to a silica waveguide grating router," *IEEE Photon. Technol. Lett.*, vol. 15, no. 10, pp. 1446–1448, Oct. 2003.
- [3] Z. Zhu, M. Funabashi, Z. Pan, L. Paraschis, and S. J. B. Yoo, "1000 cascaded stages of optical 3R regeneration with SOA-MZI-based clock enhancement to achieve 10-Gb/s 125 000-Km dispersion uncompensated transmission," *IEEE Photon. Technol. Lett.*, vol. 18, no. 10, pp. 2159–2161, Oct. 2006.
- [4] J. Y. Kim, J. M. Kang, T. Y. Kim, and S. K. Han, "All-optical multiple logic gates with XOR, NOR, OR, and nand functions using parallel SOA-MZI structures: Theory and experiment," *J. Lightw. Technol.*, vol. 24, no. 9, pp. 3392–3399, Sep. 2006.
- [5] M. Matsuura, N. Kishi, and T. Miki, "All-optical wavelength conversion with large wavelength hopping by utilizing multistage cascaded SOA-based wavelength converters," *IEEE Photon. Technol. Lett.*, vol. 18, no. 4, pp. 926–928, Apr. 2006.
- [6] S. B. Kuntze, L. Pavel, and J. S. Aitchison, "Controlling a semiconductor optical amplifier using a state-space model," *IEEE J. Quantum Electron.*, vol. 43, no. 2, pp. 123–129, Feb. 2007.
- [7] J. Gurfinkel, D. Sadot, and M. Glick, "Dynamic control analysis for semiconductor optical amplifier dynamics in optical network applications," *Opt. Eng.*, vol. 46, no. 3, p. 035004, Mar. 2007.
- [8] Y. Li, C. Wu, S. Fu, P. Shum, Y. Gong, and L. Zhang, "Power equalization for SOA-based dual-loop optical buffer by optical control pulse optimization," *J. Lightw. Technol.*, vol. 43, no. 6, pp. 508–516, Jun. 2007.
- [9] C. Michie, A. E. Kelly, I. Armstrong, I. Andonovic, and C. Tombling, "An adjustable gain-clamped semiconductor optical amplifier (AGC-SOA)," *J. Lightw. Technol.*, vol. 25, no. 6, pp. 1466–1473, Jun. 2007.
- [10] F. Tabatabai and H. S. Al-Raweshidy, "Feedforward linearization technique for reducing nonlinearity in semiconductor optical amplifier," *J. Lightw. Technol.*, vol. 25, no. 9, pp. 2667–2674, Sep. 2007.
- [11] W. Mathlouthi, P. Lemieux, M. Salsi, A. Vannucci, A. Bononi, and L. A. Rusch, "Fast and efficient dynamic {WDM} semiconductor optical amplifier model," *J. Lightw. Technol.*, vol. 24, no. 11, pp. 4353–4365, Nov. 2006.
- [12] S. Skogestad and I. Postlethwaite, *Multivariable Feedback Control*, 2nd ed. New York: Wiley, 2005.
- [13] J. Huang and L. W. Casperson, "Gain and saturation in semiconductor lasers," *Opt. Quantum Electron.*, vol. 25, pp. 369–390, 1993.
- [14] H. M. Salgado, J. C. S. Castro, and J. J. O'Reilly, "Effect of gain compression on the FM nonlinear distortion in semiconductor lasers," *IEEE J. Quantum Electron.*, vol. 32, no. 6, pp. 981–985, Jun. 1996.
- [15] J. M. Tang, P. S. Spencer, and K. A. Shore, "Influence of fast gain depletion on the dynamic response of toad's," *J. Lightw. Technol.*, vol. 16, no. 1, pp. 86–91, Jan. 1998.
- [16] H. Shi, "Performance analysis on semiconductor laser amplifier loop mirrors," *J. Lightw. Technol.*, vol. 20, no. 4, pp. 682–688, Apr. 2002.
- [17] E. Conforti, C. M. Gallep, S. H. Ho, A. C. Bordonalli, and S.-M. S. Kang, "Carrier reuse with gain compression and feed-forward semiconductor optical amplifiers," *IEEE Trans. Microw. Theory Technol.*, vol. 50, no. 1, pp. 77–81, Jan. 2002.
- [18] S. H. Kim, J. H. Kim, B. G. Yu, Y. T. Byun, Y. M. Jeon, S. Lee, and D. H. Woo, "All-optical nand gate using cross-gain modulation in semiconductor optical amplifiers," *Electron. Lett.*, vol. 41, pp. 1027–1028, Sep. 2005.
- [19] G. Contestabile, R. Proietti, N. Calabretta, and E. Ciaramella, "Cross-gain compression in semiconductor optical amplifiers," *J. Lightw. Technol.*, vol. 25, no. 3, pp. 915–921, Mar. 2007.
- [20] M. Willatzen, A. Uskov, J. Mørk, H. Olesen, B. Tromborg, and A.-P. Jauho, "Nonlinear gain suppression in semiconductor lasers due to carrier heating," *IEEE Photon. Technol. Lett.*, vol. 3, no. 7, pp. 606–609, Jul. 1991.
- [21] A. Mecozzi and J. Mørk, "Saturation induced by picosecond pulses in semiconductor optical amplifiers," *J. Opt. Soc. Amer. B, Opt. Phys.*, vol. 14, no. 4, pp. 761–770, Apr. 1997.
- [22] M. J. Connelly, "Wideband semiconductor optical amplifier steady-state numerical model," *IEEE J. Quantum Electron.*, vol. 37, no. 3, pp. 439–447, Mar. 2001.
- [23] L. Thylén, "Amplified spontaneous emission and gain characteristics of fabry-perot and traveling wave type semiconductor laser amplifiers," *IEEE J. Quantum Electron.*, vol. 24, no. 8, pp. 1532–1537, Aug. 1988.
- [24] L. A. Coldren and S. W. Corzine, *Diode Lasers and Photonic Integrated Circuits*. New York: Wiley, 1995.
- [25] A. Mecozzi, S. Scotti, A. D'Ottavi, E. Iannone, and P. Spano, "Four-wave mixing in traveling-wave semiconductor amplifiers," *IEEE J. Quantum Electron.*, vol. 31, no. 4, pp. 689–699, Apr. 1995.
- [26] A. J. Zilkie, J. Meier, P. W. E. Smith, M. Mojahedi, J. S. Aitchison, P. J. Poole, C. N. Allen, P. Barrios, and D. Poitras, "Femtosecond gain and index dynamics in an InAs/InGaAsP quantum dot amplifier operating at 1.55 μm ," *Opt. Express*, vol. 14, no. 4, pp. 11453–11459, Nov. 2006.
- [27] A. J. Zilkie, J. Meier, M. Mojahedi, P. J. Poole, P. Barrios, D. Poitras, T. J. Rotter, C. Yang, A. Stintz, K. J. Mallow, P. W. E. Smith, and J. S. Aitchison, "Carrier dynamics of quantum dot, quantum dash, and quantum well semiconductor optical amplifiers operating at 1.55 μm ," *IEEE J. Quantum Electron.*, vol. 43, no. 11, pp. 982–991, Nov. 2007.
- [28] D. Ban, E. H. Sargent, K. Hinzler, S. J. Dixon-Warren, A. J. SpringThorpe, and J. K. White, "Direct observation of lateral current spreading in ridge waveguide lasers using scanning voltage microscopy," *Appl. Phys. Lett.*, vol. 82, no. 23, pp. 4166–4168, Jun. 2003.
- [29] J. S. Weiner, J. S. Lee, A. Leven, Y. Baeyens, V. Houtsma, G. Georgiou, Y. Yang, J. Frackowiak, A. Tate, R. Reyes, R. F. Kopf, W.-J. Sung, N. G. Weimann, and Y.-K. Chen, "An InGaAs-InP HBT differential transimpedance amplifier with 47-GHz bandwidth," *IEEE J. Solid-State Circuits*, vol. 39, no. 10, pp. 1720–1723, Oct. 2004.

Scott B. Kuntze received the B.Sc.Eng. degree in mathematics and engineering from Queen's University, Kingston, ON, Canada, in 2002 and the M.A.Sc. degree in electrical engineering (photonics) from the University of Toronto, Toronto, ON, Canada, in 2004, where he is currently working towards the Ph.D. degree in photonics in the Department of Electrical and Computer Engineering.

He spent internships working in the Advanced Technology Investments Department at Nortel Networks building next-generation photonic transceivers and switches from 2000 to 2001, and in the High Performance Optical Components Division at Nortel studying semiconductor lasers using novel probing techniques in 2002. His current research interests include the robust analysis, design, and control of active integrated photonic devices using control theory. He is funded by a NSERC Canadian Graduate Scholarship.

Aaron J. Zilkie (S'98–M'07) was born in Winnipeg, MB, Canada, in 1978. He received the B.Sc. degree in electrical engineering from the University of Manitoba, Winnipeg, MB, Canada, in 2001 and the M.A.Sc. degree in electrical and computer engineering from the University of Toronto, Toronto, ON, Canada, where he is currently working towards the Ph.D. degree in electrical and computer engineering.

He interned at Nortel Networks, Ottawa, ON, Canada, from 1999 to 2000, in the optical networks division before beginning his M.A.Sc. degree. His current research interests include semiconductor quantum dot devices, semiconductor optical amplifiers for all-optical switching, and nonlinear processes in semiconductor materials and their applications.

Mr. Zilkie is a student member of the Optical Society of America (OSA).

Lacra Pavel (S'93–M'96–SM'04) received the Ph.D. degree in electrical engineering from Queen's University, Kingston, ON, Canada, in 1996, with a dissertation on nonlinear H-infinity control.

She spent a year at the Institute for Aerospace Research (NRC) in Ottawa as a NSERC Postdoctoral Fellow. From 1998 to 2002, she worked in the optical communications industry at the frontier between systems control, signal processing, and photonics. She joined the University of Toronto, Toronto, ON, Canada, in August 2002, as an Assistant Professor in Electrical and Computer Engineering Department. Her research interests include: system control and optimization in optical networks, game theory, robust and H-infinity optimal control, real-time control and applications.

Dr. Pavel was an Associate Editor, Member on the Program Committee of IEEE Control Applications Conference 2005; Associate Chair (Control) on the Program Committee of IEEE Canadian Conference of Electrical and Computer Engineering 2004. She is a member of CSS/ComSoc/LEOS and member of Optical Society of America (OSA).

J. Stewart Aitchison (M'96–SM'00) received the B.Sc. (with first class honors) and Ph.D. degrees from the Physics Department, Heriot-Watt University, Edinburgh, U.K., in 1984 and 1987, respectively. His dissertation research was on optical bistability in semiconductor waveguides.

From 1988 to 1990, he was a Postdoctoral Member of Technical Staff at Bellcore, Red Bank, NJ. His research interests were in high nonlinearity glasses and spatial optical solitons. He then joined the Department of Electronics and Electrical Engineering, University of Glasgow, U.K., in 1990 and was promoted to a personal chair as Professor of Photonics in 1999. His research was focused on the use of the half band gap nonlinearity of III–V semiconductors for the realization of all-optical switching devices and the study of spatial soliton effects. He also worked on the development of quasi-phase matching techniques in III–V semiconductors, monolithic integration, optical rectification, and planar silica technology. His research group developed novel optical biosensors, waveguide

lasers and photosensitive direct writing processes based around the use of flame hydrolysis deposited (FHD) silica. In 1996, he was the holder of a Royal Society of Edinburgh Personal Fellowship and carried out research on spatial solitons as a visiting researcher at CREOL, University of Central Florida. Since 2001, he has held the Nortel chair in Emerging Technology, in the Department of Electrical and Computer Engineering, University of Toronto, Toronto, ON, Canada. His research interests cover all-optical switching and signal processing, optoelectronic integration, and optical biosensors. His research has resulted in seven patents, around 185 journal publications, and 200 conference publications. From 2004 to 2007, he was the Director of the Emerging Communications Technology Institute at the University of Toronto. Since 2007, he has been vice Dean Research, for the Faculty of Applied Science and Engineering, University of Toronto.

Dr. Aitchison is a Fellow of the Optical Society of America and a Fellow of the Institute of Physics London.